A Computational Study of Direct CO_2 Hydrogenation to Methanol on Pd Catalysts

Igor Kowalec [a], Lara Kabalan [a], C. Richard A. Catlow [a,b,c] and Andrew J. Logsdail [a,*]

[a] Cardiff Catalysis Institute, School of Chemistry, Cardiff University, Cardiff, United Kingdom

[b] UK Catalysis Hub, Research Complex at Harwell, RAL, Oxford, OX11 0FA, United Kingdom

[c] Department of Chemistry, University College London, London, WC1H 0AJ, United Kingdom

[*] Email: LogsdailA@cardiff.ac.uk

Abstract

We investigate the mechanism of direct CO_2 hydrogenation to methanol on Pd (111), (100) and (110) surfaces using density functional theory (DFT), providing insight into the reactivity of CO_2 on Pd-based catalysts. The initial chemisorption of CO_2, forming a partially charged $CO_2^{\delta-}$, is weakly endothermic on a Pd (111) surface, with an adsorption energy of 0.06 eV, and slightly exothermic on Pd (100) and (110) surfaces, with adsorption energies of -0.13 and -0.23 eV, respectively. Based on Mulliken analysis, we attribute the low stability of $CO_2^{\delta-}$ on the Pd (111) surface to a negative charge that accumulates on the surface Pd atoms interacting directly with the $CO_2^{\delta-}$ adsorbate. For the reaction of the adsorbed species on the Pd surface, HCOOH hydrogenation to H_2COOH is predicted to be the rate determining step of the conversion to methanol in all cases, with activation barriers of 1.35, 1.26, and 0.92 eV on Pd (111), (100) and (110) surfaces, respectively.

1. Introduction

Methanol synthesis by direct hydrogenation of CO_2 has been recognised as a potential route towards sustainable fuels for transport and a circular fuel economy.[1] The most efficient commercialised catalyst for methanol synthesis is the heterogeneous mixture of copper oxide (CuO), zinc oxide (ZnO) and alumina (Al_2O_3), abbreviated as CZA, which is designed for use with syngas feedstock, itself a product of coal gasification and steam reforming.[2] Initially, CZA was proposed to facilitate decomposition of the CO_2 present in the feedstock to CO, *via* the reverse water-gas shift (RWGS) reaction, and then subsequent hydrogenation leads to CH_3OH, where low concentrations of CO_2 ensure the required surface oxidation level; however, in a mechanistic study using ^{14}C isotope-labelled reactants, Chinchen *et al.* revealed that CO_2, and not CO, is likely to be the main source of carbon in methanol synthesised from $CO/CO_2/H_2$ mixtures.[3,4] CZA is inefficient with a pure CO_2 feedstock and, at relatively high concentrations in syngas, CO_2 acts as a poison by adhering to the surface strongly and occupying the reaction sites.[3]

Methanol synthesis from fossil fuels is efficient and profitable, but environmental pressures are urging the chemical industry to transfer from a linear-oil economy to net zero emissions by 2050.[5] One such strategy can be direct CO_2 hydrogenation to methanol, but a better understanding of the CO_2 interaction with transition metal catalysts is required for the design of novel catalytic materials. Many factors, such as the source of H_2 , affect the extent to which the process of direct methanol synthesis from CO_2 can be "green"; however, the idea of using of an atmospheric pollutant such as anthropogenic CO_2 for fuel synthesis, and/or also generating feedstock for further synthesis of chemical compounds, such as formic acid, is broadly appealing.[6]

1.1 CO_2 activation

A crucial step in the direct hydrogenation of CO_2 to methanol is the initial CO_2 activation. On a heterogeneous catalyst, the RWGS reaction needs to be inhibited while maintaining a strong interaction between CO_2 and the catalytic surface.[6,7] Pd alone exhibits poor selectivity to methanol for direct CO_2 hydrogenation, but the selectivity is greatly enhanced when it is alloyed with other transition metals, such as Zn.[6] In order to understand fully the Pd-based alloy reactivity, it is necessary first to know the nature of interactions between CO_2 and Pd. The available experimental data for the interaction of CO_2 with Pd facets is limited, but computation using density functional theory (DFT) is providing insight into the processes.[8–11] Burghaus *et al.* reported that CO_2 reactivity on clean Pd surfaces is weak, not favouring dissociation to CO unless an alkali metal species is coadsorbed.[11] The weak interaction is considered to be predominantly a Van der Waals physisorption, based on the

theoretical and experimental observations at the Pd (111) surface.[10,12,13] CO_2 adsorption on Pd has been studied in the context of RWGS reaction and utilisation of syngas, and desorption of CO_2 from the Pd (111) surface reported as requiring 0.26 eV of energy.[10] Solymosi *et al.* reported that CO_2 desorption from the Pd (100) surface also has a relatively low energy, 0.35 eV; this was, however, associated with a chemisorption, involving a metal to empty CO_2 π* orbital electron transfer.[8] Therefore, the character of the CO_2 interaction with Pd surfaces seems to depend on the particular surface structure. The differing adsorption energies can be correlated with surface energies, as physisorption was exclusively observed on the lowest energy (111) surface, and experimental evidence of chemisorption observed for CO_2 on the higher energy Pd (100).[8–10]

Complementary to these observations, the rate for catalytic hydrogenation of CO_2 on Pd is reported as greatly increased when the active species is paired with suitable metal oxide supports, such as TiO_2 and ZnO, as they facilitate CO_2 adsorption and activation.[14–16] Ko *et al.* computationally investigated the adsorption of CO_2 on transition metal surfaces, using the PBE density functional with a DFT-D2 dispersion correction, and reported two types of CO_2 adsorption on Pd (111): an exothermic physisorption (-0.33 eV) of undistorted CO_2, parallel to the surface; and a less exothermic chemisorption (-0.18 eV) with CO_2 in a bent geometry, and having a partial negative charge.[17] In contrast, Zhang *et al.* recently computed the CO_2 chemisorption on Pd (111) to be endothermic (0.06 eV) using the PBE density functional; this is in agreement with previous studies by Habas *et al.*, who reported the adsorption energy of CO_2 to be 0.22 eV above the dissociation limit, as calculated with DFT using the B3LYP density functional.[18] Interestingly, Liu *et al.* have shown that, when using the PBE density functional, the inclusion of the Van der Waals forces *via* the DFT-D2 method dramatically changes the adsorption energy of chemisorbed species on the Pd (111) surface, from 0.30 eV to -0.18 eV.[13] Although there is no consensus on the matter of CO_2 chemisorption endo- or exothermicity on Pd surfaces, the reported values are generally low, which agrees with the experimental reports of weak interaction between CO_2 and Pd surfaces.

1.2 Mechanism of direct CO_2 hydrogenation to methanol

It has been argued that a catalyst is most likely to facilitate direct CO_2 hydrogenation to methanol via a surface formate intermediate (HCOO*, where * indicates an adsorbed species), with Medford *et al.* having shown that HCOO* could act as a poison for other reaction pathways due to its high thermodynamic stability on the catalyst surface.[19] Variations of the mechanism proposed by Grabow, which progresses via formic acid (HCOOH) as shown in Figure 1, have been proposed, such as an initial Eley-Rideal type mechanism on Cu-based catalytic systems, where CO_2 in the gas phase reacts with surface-bound hydrogen to yield formate.[20] Huš *et al.* observed that CO_2 binds to the metal surface in

a bent geometry, where one of the oxygens binds to a secondary metal atom and the carbon binds to a metal atom underneath.[21] Recently, Huš *et al.* concluded that dioxymethylene (H_2CO_2*) should be preferably considered over formic acid (HCOOH*) on Cu-based catalysts as the former is more strongly bound to the metallic surface and the activation energy towards hydroxymethoxy (H_2COOH*) is lower.[21]

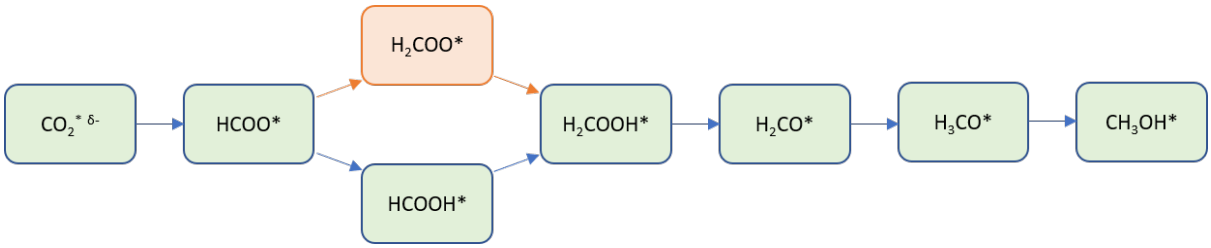

Figure 1. Formate pathway of direct CO_2 hydrogenation to methanol on metallic surfaces, as proposed by Grabow *et al.* (via HCOOH*) and Huš *et al.* (via H_2COO*). * indicates a surface-bound species and δ- indicates that CO_2 is partially charged and in a bent geometry.[21,22]

Pd-based catalysts supported on ZnO are potent alternative catalysts for this reaction, with their reactivity attributed to the Pd-Zn binary metallic phases and their stabilisation of the HCOO* intermediate, similar to the Cu-based catalyst. [15,16] Zhang *et al.* have reported DFT studies of an alternative CO_2 formate mechanism that involves dissociation of formic acid to HCO and OH, and subsequent hydrogenations of HCO to produce CH_3OH.[23] On the other hand, Brix *et al.* have recently considered the initial CO_2 hydrogenation on Pd (111) to proceed via carboxylic acid (COOH), instead of formate, in their DFT study using PBE coupled with DFT-D3 dispersion correction, and they observed a high energy barrier of 2.23 eV for CO_2 hydrogenation to formate on Pd (111), in contrast to the barrier of 0.85 eV reported by Zhang *et al*.[23,24]

Binary and ternary metallic alloy catalysts offer better selectivity, stability and tunability than their monometallic counterparts, but understanding their electronic properties and interactions with reactants becomes increasingly difficult with varying composition. Thus, in order to provide foundations for studying such systems, we present here an in-depth investigation of CO_2 interaction with low energy Pd (111), (110) and (100) surfaces using DFT calculations, followed by investigation of the direct CO_2 hydrogenation to CH_3OH, *via* the Grabow mechanism, on the Pd (111), (110) and (100) surfaces, in the context of rationalising CO_2 reactivity on Pd-based catalysts.

2. **Methodology**

The Fritz Haber Institute *ab initio* molecular simulations (FHI-aims) software package has been used for full potential all-electron DFT calculations, with the Pythonic Atomic Simulation Environment (ASE) used for management of calculation geometries.[25,26] The default convergence criteria within FHI-aims for self-consistent field (SCF) calculations were used, i.e. the changes between the current and previous SCF iterations in charge density, sum of eigenvalues and total energy were below N x 1.67 x 10^{-5} e a_0^3, 10^{-3} eV and 10^{-6} eV, respectively, where N is the number of atoms in the model. Scalar relativistic treatment of kinetic energy for all elements was achieved by the atomic zero-order regular approximation (ZORA), and a Gaussian-type broadening with width of 0.01 eV was applied to the occupation of electronic states. The Perdew-Burke-Ernzerhof exchange correlation (XC) density functional has been unless explicitly stated otherwise, paired with the Tkatchenko-Scheffler Van der Waals dispersion correction (PBE+vdW). A default "light" basis set have been used for geometry optimisations, as structural accuracy converges with this basis;[25,27,28] energy calculations were then performed with a "tight" basis set on the optimised geometries, providing greater electronic accuracy and mitigation of basis set superposition error.[25] This approach provides maximum resource efficiency, as SCF iterations with a "light" basis require ~50 % less time than with a "tight" basis set. For geometry optimisations, convergence was deemed complete when forces on all unconstrained atoms were less than 0.01 eV/Å.

Due to the closed-shell electronic configuration of Pd ([Kr] $4d^{10}$), spin-paired calculations were used in periodic calculations; gas-phase adsorbate structures were calculated both spin-paired and spin-unpaired, and the energy of the more stable system was considered for reference to periodic calculations. The effect of the spin treatment on the activation energies in relevant surface hydrogenation reactions has been assessed in Section S3 of the Supporting Information (SI), with a spin-paired treatment shown to introduce small error bars of ±0.05 eV.

2.1 Bulk models

For sampling the Brillouin zone of face-centred cubic (FCC) Pd in a primitive unit cell, a (9 × 9 × 9) Monkhorst–Pack **k**-grid was found to provide converged accuracy, as detailed in Section S1 of the SI.[29] The lattice constant (a_0 = 3.914 Å), bulk modulus (B_0 = 183.37 GPa) and cohesive energy (E_{coh} = 3.996 eV) calculated for bulk face-centred cubic (FCC) Pd match closely with the experimental observations of 3.88 Å, 180.40 GPa and 3.89 eV, respectively.[30,31]

2.2 Surface models

Using the optimised model of bulk FCC Pd, a surface supercell was created with dimensions of (3 x 3 x *n*), where *n* is the number of atomic layers in the *z*-direction perpendicular to the material surface. The *x*- and *y*-dimensions were chosen such that the adsorbates are significantly separated (7.5 Å), and a vacuum layer of 40 Å was added in the *z*-direction. The **k**-grid sampling was reduced appropriately for the introduction of the vacuum gap between slabs, maintaining reciprocal space sampling of (0.04 x 2π) $Å^{-1}$ in the *x*- and *y*-directions with a **k**-grid of (3 x 3 x 1). Due to the one-sided nature of the slab models considered, a dipole-correction was used in all calculations.

The energy penalty for breaking chemical bonds at the surface of a material (E_{cleave}) is calculated as:

$$E_{\text{cleave}} = \frac{E_{\text{Slab}}^{\text{Unrelaxed}} - N \cdot E_{\text{bulk}}}{2A} \qquad \textit{Equation 1.}$$

where the DFT total energy of a surface slab model ($E_{\text{Slab}}^{\text{Unrelaxed}}$), the bulk energy per atom (E_{bulk}), the number of atoms in the model (*N*), and the surface area (*A*), are necessary. To calculate the optimised surface energy (E_{surf}), the energy of stabilisation provided by geometry relaxation (E_{relax}) needs to be obtained from the difference in total DFT energy of the optimised slab ($E_{\text{Slab}}^{\text{Relaxed}}$) and $E_{\text{Slab}}^{\text{Unrelaxed}}$:

$$E_{\text{relax}} = \frac{E_{\text{Slab}}^{\text{Relaxed}} - E_{\text{Slab}}^{\text{Unrelaxed}}}{A} \qquad \textit{Equation 2.}$$

where here we have considered a single-sided model of the surface, hence the denominator is *A* only. The surface energy (E_{surf}) can then be calculated as follows:

$$E_{\text{surf}} = E_{\text{cleave}} + E_{\text{relax}} \qquad \textit{Equation 3.}$$

Tests of the effect of slab thickness, *n*, on E_{cleave} were performed for the Pd (111), (100) and (110) facets, where convergence of the surface energies were used as a metric of model accuracy (Figure 2). E_{cleave} converges for $n \geq 5$; thus, 5 layers are used for all subsequent calculations.

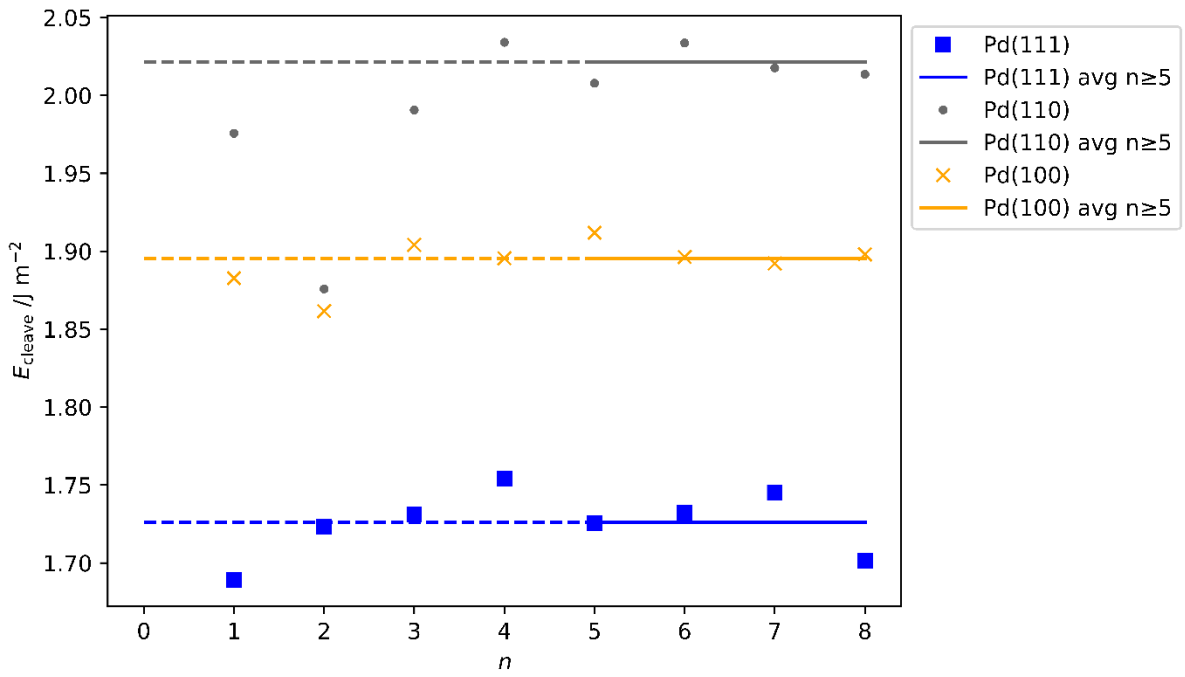

Figure 2. E_{cleave} calculated for Pd FCC (111), (110) and (100) surfaces as a function of increasing model thickness, *n*. A key is provided to identify the symbols and linear fits; the average cleave energy (solid horizontal line) was taken from $n \geq 5$, to avoid bias from inaccurate thin slabs (dashed lines).

For the slab models, constraints were used to maintain the bulk structure for Pd atoms distant from the adsorption site. These constraints were included for the bottom layers in all our one-sided models; testing for all three surface facets with the top one, two or three layers of atoms unconstrained shows that E_{relax} converges only in the calculations when the top three surface layers are unconstrained.

Thus, in summary, a 3 x 3 x 5 supercell surface model has been used herein with the bottom two layers constrained to their bulk positions, and the three top surface layers unconstrained. The surface energies (E_{surf}) with these settings are presented in Table 1. The calculated Pd (111), (100) and (110) E_{surf} match previous computation and experiments, thus supporting the validity of our approach.

Table 1. Pd FCC (111), (100) and (110) surface energies calculated using PBE+vdw and a "tight" basis set. Literature and experiment are provided for comparison.

Ref	XC	E_{surf} /(J m^{-2})		
		Pd (111)	Pd (100)	Pd (110)
This work	**PBE+vdW**	**1.72**	**1.91**	**1.99**
Methfessel *et al.*[32]	LDA	1.64	1.86	1.97
Vitos *et al.*[33]	GGA	1.92	2.33	2.23
Patra *et al.*[34]	LDA	1.88	2.43	2.25
	PBE	1.36	1.79	1.61
	PBEsol	1.63	2.15	1.93
	SCAN	1.54	2.03	1.83
	SCAN+rVV10	1.77	2.29	2.05
Singh-Miller *et al.*[35]	PBE	1.31	1.49	1.55
Da Silva *et al.*[36]	LDA	1.87	-	-
	PBE	1.33	-	-
Skriver *et al.*[37]	LDA	1.88	-	-
Tyson *et al.*[38]	Experiment	2.00	-	-
Boer *et al.*[39]	Experiment	2.01	-	-

2.3 Surface adsorption

For surface reactions, the adsorption energy (E_{ads}) measures the interaction between a catalyst and reactant, and is deduced from comparison of the energies of the optimised gas-phase adsorbate (E_A), optimised surface (E_B) and the combined system (E_{AB}).

$$E_{\text{ads}} = E_{AB} - (E_A + E_B) \qquad \textit{Equation 4.}$$

where a negative value indicates favourable adsorption. Due to basis set incompleteness when using an atom centred basis, a Boys-Bernardi counterpoise correction is necessary for surface-adsorbate interactions to account for the basis set superposition error (BSSE).[40] In our work, the BSSE for CO_2 adsorbed on Pd (111) was assessed on an aperiodic model with all Pd atoms within 7.0 Å of the adsorbed CO_2 molecule included (i.e. all atoms within the basis set cutoff, including those in neighbour cells). The energy of the CO_2 in the presence and absence of Pd basis functions ($E_{A(AB)}$ and $E_{A(A)}$, respectively) were compared, and the equivalent comparison of the energy of the slab model in the presence and absence of the basis functions of the CO_2 adsorbate ($E_{B(AB)}$ and $E_{B(B)}$, respectively) was also performed.[40] The BSSE energy (E_{BSSE}) was then calculated as:[40]

$$E_{\text{BSSE}} = \left[E_{A(AB)} - E_{A(A)}\right] + \left[E_{B(AB)} - E_{B(B)}\right] \qquad \textit{Equation 5.}$$

The more negative the E_{BSSE}, the higher the overbinding error. By subtracting E_{BSSE} from E_{ads}, the counterpoise corrected adsorption energy can be established (E_{ads}^{CP}) as:

$$E_{ads}^{CP} = E_{ads} - E_{BSSE} \qquad \textit{Equation 6.}$$

With the "light" basis set, E_{BSSE} is -0.08 eV for CO_2 on Pd (111); E_{BSSE} was reduced significantly to -0.02 eV with the "tight" basis set. Considering the low BSSE with the "tight" basis, which is used subsequently throughout this work, the E_{BSSE} contribution to E_{ads} was deemed negligible and was not calculated for species other than CO_2.

2.4 Transition state structures

For kinetic studies, we have used a machine learning nudged elastic band (MLNEB) method to identify saddle points and minimum energy paths (MEPs).[41,42] A spring constant of 0.05 eV/Å has been used throughout; the convergence criterion of forces on all unconstrained atoms of below 0.05 eV/Å, with energy uncertainty below 0.03 eV, was deemed sufficiently accurate for CO_2 adsorption. Comparison with a more stringent force criterion of 0.01 eV/Å altered the activation energy for CO_2 adsorption on FCC (111) surface by 5 meV only (Section S2, SI).

3. Results and discussions

3.1 Hydrogen adsorption

Prior to investigating the hydrogenation of CO_2 over Pd, it is crucial to gain an understanding of hydrogen behaviour on Pd. Thus, initially a survey of E_{ads} for a H atom was conducted on Pd (111), (100) and (110) surfaces. The H atom was positioned at various locations above the surface and optimised, with constraints in the *xy*-plane, until the forces on each atom were < 0.01 eV/Å. The calculated E_{ads}(H) on the Pd (111), (100), and (110) surfaces, with respect to the gas-phase diatomic hydrogen molecule, are plotted as a function of *x*- and *y*- coordinate in Figure 3(i), 4(i), and 5(i), respectively, which allows visual inspection of hydrogen atom stability on these surfaces.

The most stable adsorption site for the H atom on the Pd (111) surface is the HCP hollow position, which is site B in Figure 3(ii), with E_{ads}(H) of -0.67 eV; similar stability over high coordination sites is observed on the (100) surface, where the hollow site (Figure 4(ii), site C) is preferred with E_{ads}(H) of -0.54 eV, and the "FCC" site (Figure 5(ii), site B) is preferred in the case of the (110) surface, with E_{ads}(H) of -0.56 eV. The least stable adsorption sites for H atom on Pd (111), (100) and (110) facets are all atop, with E_{ads}(H) of -0.12, -0.08 and 0.00 eV, respectively. The typical reactant feed for CO_2 hydrogenation is between 1:3 to 1:9 molar ratio of CO_2 and H_2, and the dissociated hydrogen is assumed to be readily available on the catalyst surface over the course of reaction.[15,16] High hydrogen mobility can be deduced from Figure 3(i), 4(i), and 5(i), as differences in E_{ads} are low across the surfaces along specific channels, as highlighted in red. The adsorption energies for a H atom on the Pd (111) surface (-0.67 eV) and the (110) surface (-0.56 eV) compare reasonably well with the experimental work of Conrad *et al.,* who report initial heats of adsorption for ½ H_2 of 0.45 and 0.53 eV for Pd (111) and (110) surfaces, respectively.[43]

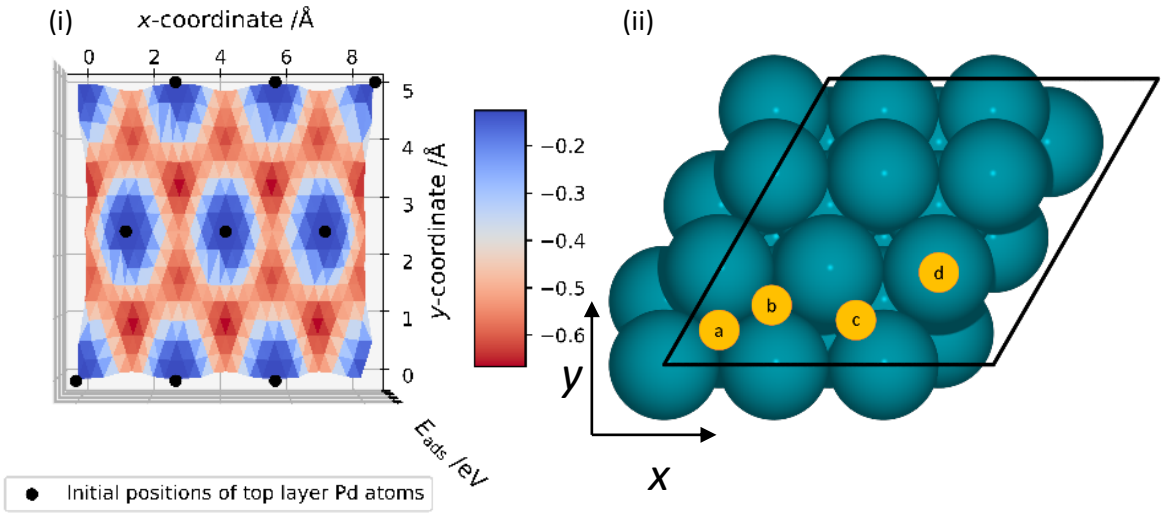

Figure 3. (i) Adsorption energy (E_{ads}) of a hydrogen atom on Pd (111) surface, calculated as a function of *x*- and *y*-coordinate; the H atom remained constrained in the *xy*-plane during each geometry optimisation. A key is provided for the adsorption energies, in units of eV. (ii) Top-down view of the FCC Pd (111) surface with a 3 x 3 x 5 atoms simulation cell. Blue spheres represent Pd atoms and yellow circles represent unique adsorption sites: a) hollow-FCC, b) hollow-HCP, c) bridge, d) atop. Black lines represent the *x*- and *y*-direction cell boundaries.

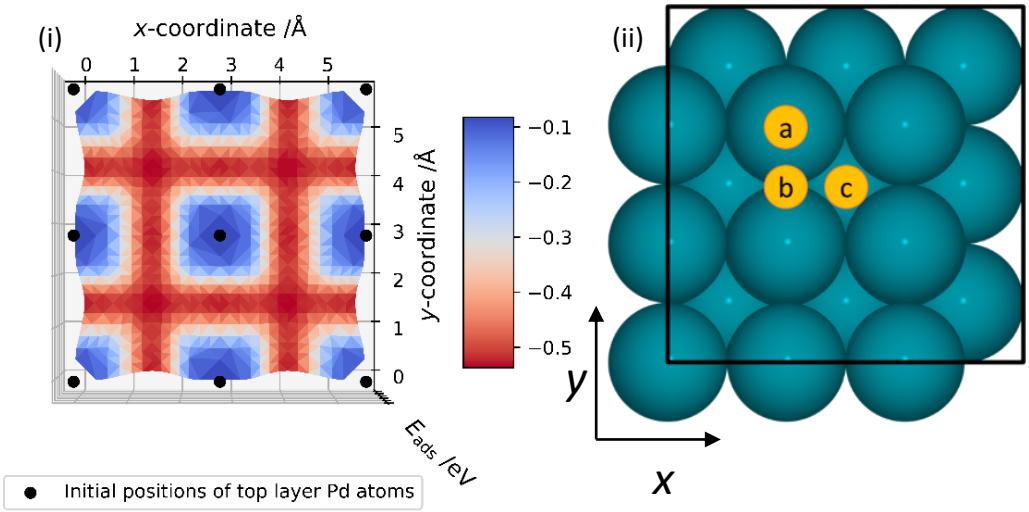

Figure 4. (i) Adsorption energy (E_{ads}) of hydrogen atom on Pd (100) surface calculated as a function of *x*- and *y*-coordinate; the H atom remained constrained in the *xy*-plane during each geometry optimisation. A key is provided for the adsorption energies, in units of eV. (ii) Top-down view of the FCC Pd (100) surface with a 3 x 3 x 5 atoms simulation cell. Blue spheres represent Pd atoms and yellow circles represent unique adsorption sites: a) atop, b) bridge c) hollow. Black lines represent the *x*- and *y*-direction cell boundaries.

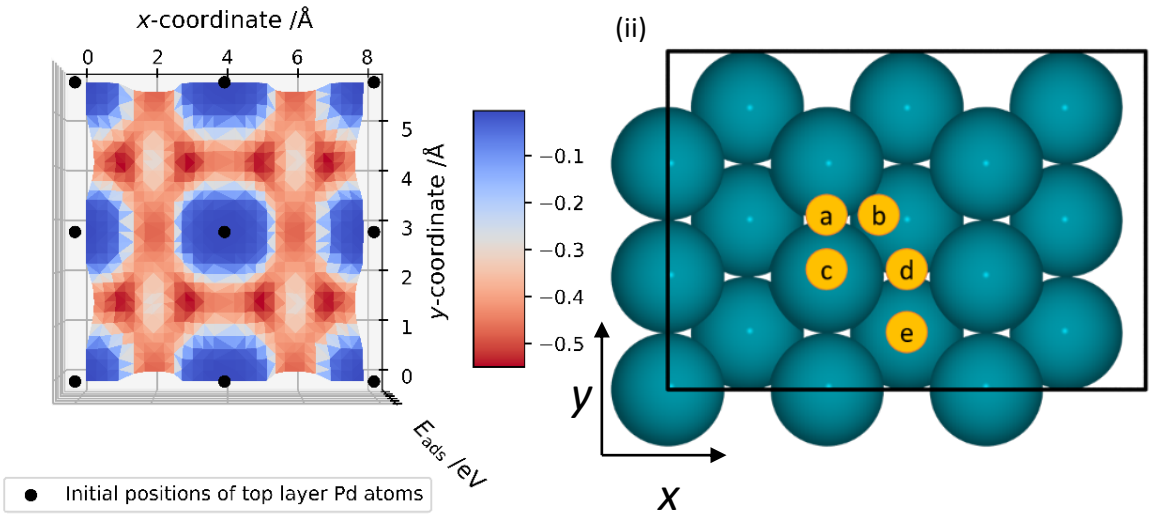

Figure 5. (i) Adsorption energy (E_{ads}) of hydrogen atom on Pd (111) surface calculated as a function of x- and y-coordinate; the H atom remained constrained in the *xy*-plane during each geometry optimisation. A key is provided for the adsorption energies, in units of eV. (ii) Top-down view of the FCC Pd (110) surface with a 3 x 3 x 5 atoms simulation cell. Blue spheres represent Pd atoms and yellow circles represent unique adsorption sites: a) short bridge, b) "FCC" c) atop, d) long bridge, e) hollow. Black lines represent the *x*- and *y*-direction cell boundaries.

3.2 CO_2 adsorption

The results of our calculations for CO_2 on the Pd (111) surface are reported in Table 2. The undistorted CO_2 is most stable with a C-Pd bond distance, $d_{(C\text{-}Pd)}$, of 3.454 Å, which agrees with the physisorbed species observed by Habas *et al.*[18] $E_{ads}(CO_2)$ is strongest on the close-packed (111) surface, and is found to relate linearly with the number of Pd atoms that neighbour the surface adsorption site; when $E_{ads}(CO_2)$ is plotted as a function of surface atom coordination number, which are 9, 8, and 7 for the Pd (111), (100), and (110) surfaces, respectively, a linear fit returns an R^2 of 0.998.

The stronger physisorption, rather than chemisorption, that we calculate for CO_2 on the Pd (111) surface was reported previously by Ko *et al.*[18] They calculated $E_{ads}(CO_2)$ of -0.33 eV for the CO_2 physisorbed on Pd (111), which is similar to the -0.21 eV calculated here; they also identify a chemisorbed state $CO_2^{\delta-}$ with E_{ads} of -0.16 eV,[17] which again is obtained here with $E_{ads}(CO_2^{\delta-})$ of 0.06 eV. The greater stability of the physisorbed CO_2 implies that there is an energy barrier on the Pd (111) surface for the activation of CO_2. Energy differences between our results and those of Ko *et al*. are likely due to small differences in the van der Waals correction, with the semiempirical DFT-D2 method of Grimme applied in the work of Ko *et al.*;[17] overall, we emphasise that the observed trends are very similar.

Table 2. Data on CO_2 and $CO_2^{\delta-}$ physisorbed and chemisorbed species on low-index Pd surfaces, respectively; CO_2^{TS} is the transition state geometry between these stable local minima. E_{ads} is the species adsorption energy, given in eV; $d_{(C-Pd^1)}$ is the distance between the carbon and the nearest neighbouring Pd given in Å, and $\angle_{O\text{-}C\text{-}O}$ is the angle between the oxygen, carbon and oxygen, given in °.

	Pd surface								
	111			100			110		
Species	E_{ads}	$d_{(C-Pd^1)}$	$\angle_{O\text{-}C\text{-}O}$	E_{ads}	$d_{(C-Pd^1)}$	$\angle_{O\text{-}C\text{-}O}$	E_{ads}	$d_{(C-Pd^1)}$	$\angle_{O\text{-}C\text{-}O}$
CO_2	-0.21	3.45	179.5	-0.18	3.28	179.1	-0.16	3.26	179.2
CO_2^{TS}	0.09	2.37	154.8	-0.02	2.45	160.6	No energy barrier		
$CO_2^{\delta-}$	0.06	2.10	140.3	-0.13	2.06	140.6	-0.23	2.06	140.2

$E_{ads}(CO_2^{\delta-})$ is endothermic (0.06 eV) on the Pd (111) surface and exothermic (-0.13 and -0.23 eV) on the Pd (100) and (110) surfaces; $E_{ads}(CO_2^{\delta-})$ on the Pd (111) surface matches that calculated by Zhang *et al.* in a similar study using the PBE XC functional.[23] It is noted that $E_{ads}(CO_2^{\delta-})$ is increasingly negative (i.e. strengthens) with increasing E_{surf} of the Pd facets, and the energy difference between surface-bound CO_2 and $CO_2^{\delta-}$ also decreases; these observations agree with experimental data that show an absence of chemisorption on the Pd (111) surface, and both physisorption and chemisorption on the Pd (100) surface.[8–10] Despite differences in $E_{ads}(CO_2^{\delta-})$ on the considered surfaces, the adsorbed geometries of CO_2 and $CO_2^{\delta-}$ are consistent across all considered surfaces (Table 2); only a small

differences in angles (0.4°) exists for either the physisorbed or chemisorbed geometries when compared across the three facets.

Mulliken charge analysis of the CO_2 and $CO_2^{\delta-}$ species adsorbed on the Pd (111), (110) and (100) facets provides insight into the electronic charge of surface species, and the data acquired are reported in Table 3. The notation used for describing charges on atoms of interest is shown in Figure 6: O^1 and O^2 are oxygen atoms on CO_2 molecule; the two closest Pd atoms interacting with CO_2 are labelled Pd^1 and Pd^2, where Pd^1 is closest to O^1 and Pd^2 is closest to O^2; and Pd_{surf}, $Pd_{sublayer}$, and Pd_{slab} refer to the first, second and all layers of Pd atoms in the model, respectively.

Table 3. Net Mulliken charges, in units of e, on relevant atoms for CO_2 physisorption and chemisorption on the Pd (111), (110) and (100) surfaces; the charges (q) have been averaged over Pd atoms in the first surface layer surface (Pd_{surf}) and sublayer ($Pd_{sublayer}$), as well as over the whole slab (Pd_{slab}).

	CO_2				$CO_2^{\delta-}$		
	Gas	Pd (111)	Pd (110)	Pd (100)	Pd (111)	Pd (110)	Pd (100)
q_C	+0.48	+0.47	+0.45	+0.44	+0.39	+0.38	+0.38
q_{O^1}	-0.24	-0.22	-0.22	-0.22	-0.19	-0.26	-0.23
q_{O^2}	-0.24	-0.23	-0.22	-0.22	-0.23	-0.24	-0.25
q_{Pd^1}	-	-0.02	-0.05	-0.05	-0.32	-0.10	-0.15
q_{Pd^2}	-	-0.01	-0.02	0.00	-0.30	+0.04	-0.07
$q_{Pd_{sublayer}}$	-	+0.02	+0.05	0.00	-0.02	+0.03	+0.00
$q_{Pd_{surf}}$	-	-0.00	-0.01	0.00	-0.07	+0.00	-0.02
$q_{Pd_{slab}}$	-	-0.02	-0.01	0.00	+0.04	+0.11	+0.10

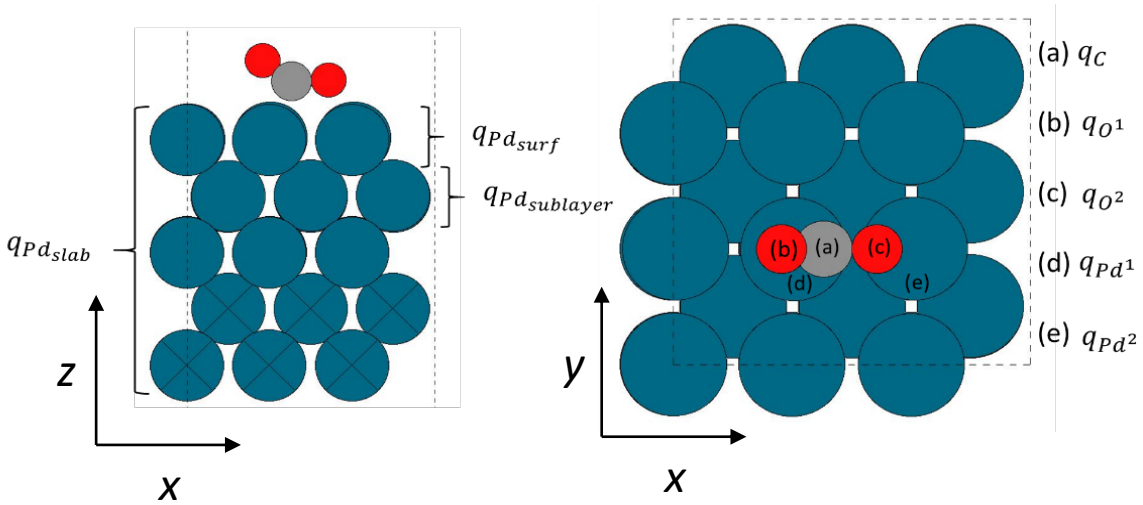

Figure 6. Side- and top-view of CO_2 chemisorbed on the FCC Pd (100) surface, illustrating notations used for Mulliken analysis. Blue, red, and grey spheres represent Pd, O, and C atoms, respectively. Black crosses mark constrained bulk Pd layers, and dashed lines illustrate the boundary of the surface supercell.

For CO_2 physisorption on the Pd (111) surface (Figure 7a), the charge of the carbon (q_C) is +0.47 e, very similar to the gas phase CO_2 (q_C = +0.48 e), and only small changes are observed on the surface Pd. For $CO_2^{\delta-}$ on the Pd (111) surface (Figure 7b), negatively charged Pd atoms bond to an oxygen and carbon (q_{Pd^1} = -0.30 e, q_{Pd^2} = -0.32 e). The distance $d_{(C-Pd^2)}$ is 2.85 Å, and there is a direct electronic interaction between Pd^2 and the carbon atom of CO_2. For chemisorbed $CO_2^{\delta-}$, the overall charge on the second layer of Pd atoms, $q_{Pd_{sublayer}}$, decreases from +0.14 to -0.15 e, whereas the charge on the first surface atomic layer of Pd, $q_{Pd_{surf}}$, has changed from -0.02 to -0.66 e, suggesting that the electron density has been pulled to the first two layers of Pd, and to the $CO_2^{\delta-}$ adsorbate *via* Pd^1 and Pd^2. q_C has decreased from +0.47 e to +0.39 e, indicating some metal (Pd^1) to empty CO_2 π* orbital electron transfer.[8] The negatively charged oxygen in proximity to the negative q_{Pd^1} and q_{Pd^2} will result in electrostatic Pauli repulsion, and thus are likely to contribute in the decreased stability of $CO_2^{\delta-}$ on the Pd (111) surface.[18,44]

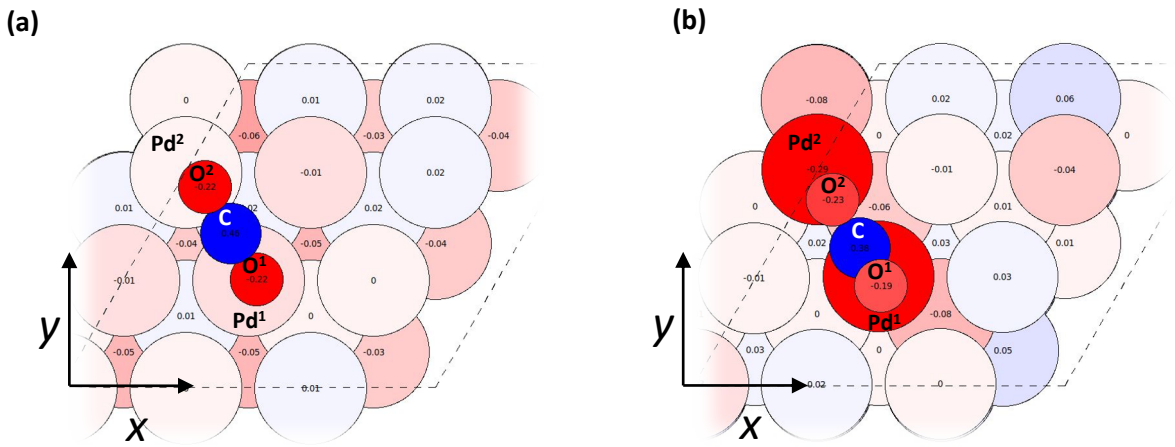

Figure 7. A red-white-blue (negative-neutral-positive charges) color-coded visualisation of the net Mulliken charge on atoms for (a) CO_2 physisorbed and (b) $CO_2^{\delta-}$ chemisorbed on the Pd (111) surface.

In contrast, for CO_2 physisorbed on the Pd (110) surface (Figure 8), q_C = +0.45 e, and, as less atoms interact with the adsorbate *via* weak Van der Waals forces, the structure is less stable than on Pd (111) by 0.05 eV. For $CO_2^{\delta-}$ on Pd (110), q_C reduces to +0.38 e, similar to for the (111) surface, though with a higher electron density on the oxygens that contributes to the overall stability (i.e. lower E_{ads}). Significantly for the (110) surface, only Pd^1, which is directly below the CO_2 carbon, is negatively charged (q_{Pd^1} = -0.10 e), demonstrating much lesser charge redistribution than on the Pd (111) surface. The differing charge transfer provides insight as to why the $CO_2^{\delta-}$ on the Pd (110) surface is more stable than on Pd (111).

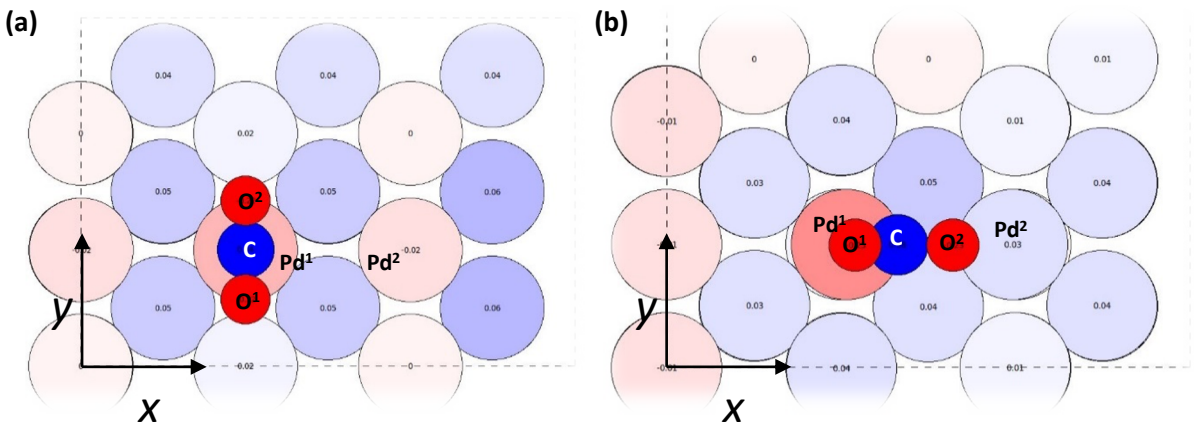

Figure 8. A red-white-blue (negative-neutral-positive charges) color-coded visualisation of the net Mulliken charge on atoms for (a) CO_2 and (b) $CO_2^{\delta-}$ on the Pd (110) surface.

For $CO_2^{\delta-}$ on a Pd (100) facet (Figure 9), the charges calculated are intermediary to the results on the Pd (111) and (110) surfaces: E_{ads} of chemisorbed $CO_2^{\delta-}$ and physisorbed CO_2 on Pd (100) are similar; and a negative charge accumulates on the carbon-bound Pd (q_{Pd^1} = -0.15 e), with a small negative charge on the oxygen-bound Pd (q_{Pd^2} = -0.07 e). The coordination of Pd (100) surface atoms is lower than that of atoms on the Pd (111) surface, which results in lower stability for the physisorbed CO_2.

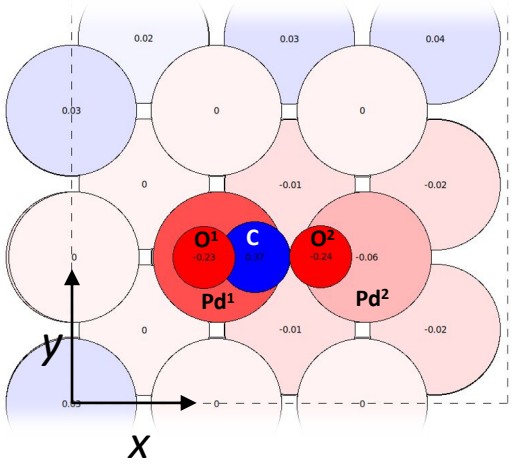

Figure 9. A red-white-blue (negative-neutral-positive charges) color-coded visualisation of the net Mulliken charge on atoms for the $CO_2^{\delta-}$ on the Pd (100) surface.

3.3 Interactions of intermediates with Pd surfaces.

Reaction intermediates from the Grabow mechanism, as introduced in Section 1.2, have been optimised on the pristine Pd (111), (100) and (110) surfaces, in each case starting from an atop position. The calculated values of E_{ads} are presented in Figure 10.

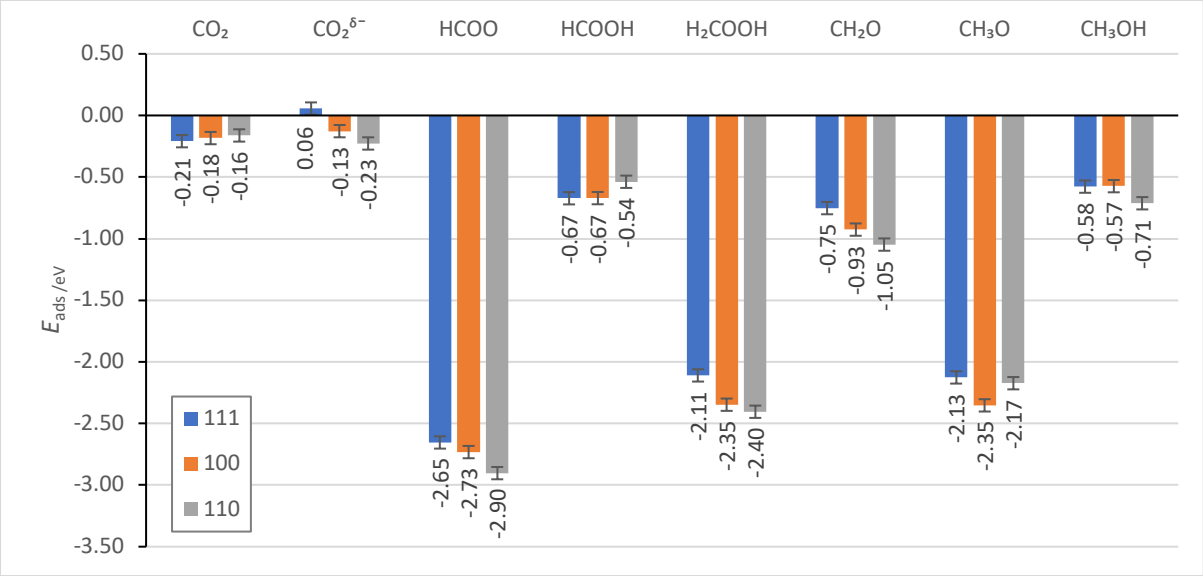

Figure 10. E_{ads} of the intermediates in the direct CO_2 hydrogenation to methanol, as studied on the low-index Pd surfaces, presented in order of increasing E_{surf}: (111), (100) and (110),[22] in blue, orange and grey, respectively. Error bars of ± 0.05 eV are provided to account for the spin-paired approximation applied to the adsorbed species, as described in Section 2.3.

For the intermediates considered, the average difference between the highest and lowest E_{ads} across the three surfaces is 0.23 eV; the lowest difference is for the HCOOH and CH_3OH molecules (0.13 and 0.14 eV, respectively), and the highest for H_2CO (0.30 eV). Plotting the surface energy (E_{surf}) of the low-index Pd surfaces against the adsorption energy (E_{ads}) of these intermediates on the corresponding surfaces (Figure 11) illustrates how trends in surface properties associate with the observations. In particular, E_{ads} of $CO_2^{\delta-}$, HCOO, H_2COOH and H_2CO present clear linear correlations with the stability of the surface facets, giving R^2 of 0.997, 0.823, 0.986 and 0.986, respectively. HCOOH, H_3CO and CH_3OH give a poor linear fit, which indicates that other factors, such as steric or electronic effects, should be considered for rationalising the strength of these adsorbate interactions with the Pd surfaces. For example, due to additional space on the long-bridge site on the Pd (110) surface, the HCOOH can be accommodated in a different orientation from that on the Pd (111) and (100) surfaces (i. e. C-H atoms facing down, rather than up), which makes the resulting structures more difficult to compare directly.

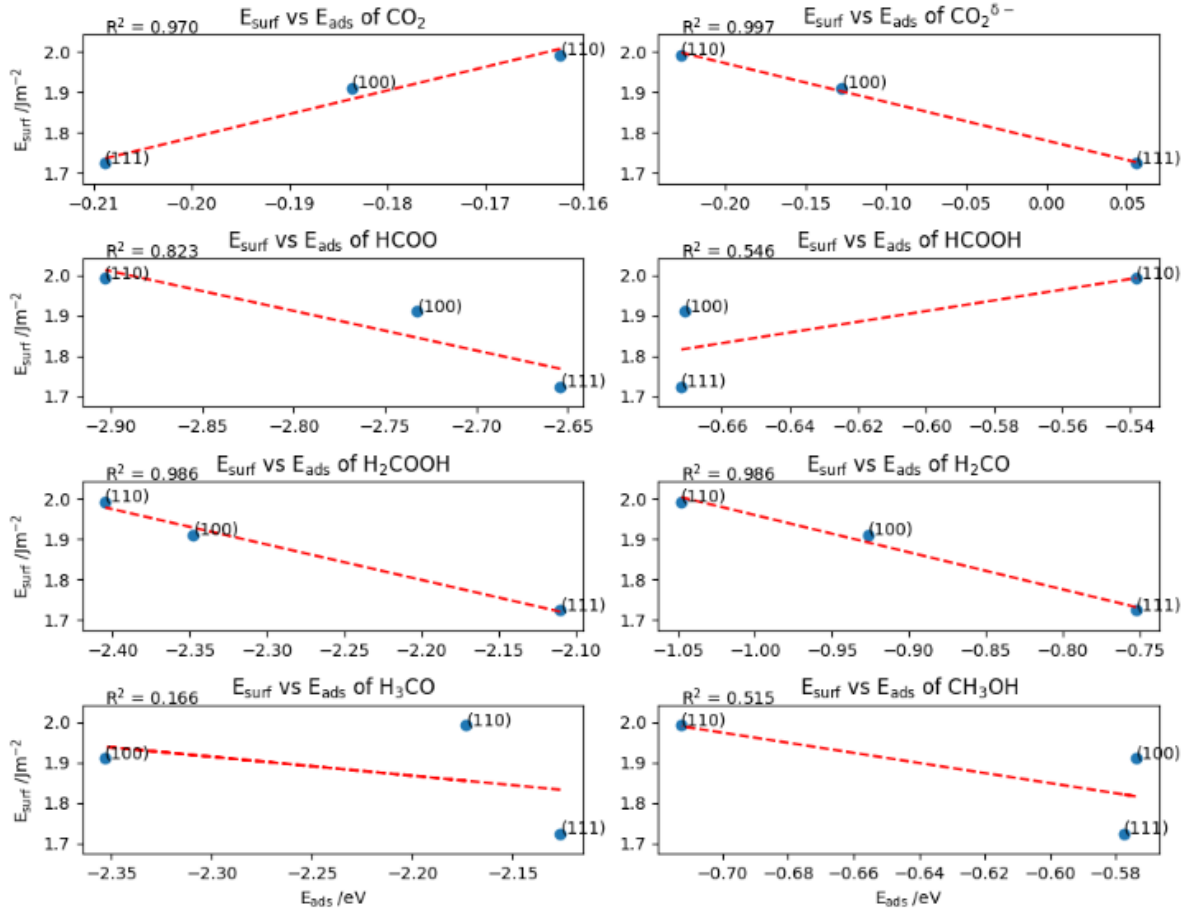

Figure 11. E_{surf} of the Pd (111), (100) and (110) surfaces plotted against E_{ads} of intermediates in the mechanism of CO_2 hydrogenation to methanol. The red dashed line is the linear fit of the data points, and R^2 is the linear coefficient of determination showing the quality of the fit.

3.4 Transition states and reaction profile

In order to determine reaction kinetics, activation energies were calculated. Here, for each reaction step that involved a hydrogenation, it was necessary to set the transition state (TS) starting geometry such that a hydrogen atom was positioned near to the intermediate; optimisation of these starting models with proximal hydrogen lead in some instances to instability of the intermediate adsorption structures, though did not cause issues when directly applied to the TS calculations. Once a transition state structure was confirmed, the activation energy (E_{act}) was calculated for each reaction step as:

$$E_{\mathrm{act}} = E_{\mathrm{TS}}\,(species) - E_{\mathrm{ads}}\,(species) \qquad \textit{Equation 7.}$$

The resulting E_{act} are presented in Figure 12, and tabulated in the SI. Here, $CO_2^{\delta-}$ was used as a reference starting point, i.e. proceeding via a Langmuir-Hinshelwood mechanism, and *not* a physisorbed CO_2 akin to an Eley-Rideal mechanism.[22] As part of the reaction pathway via formate, the decomposition of H_2COOH* into H_2CO* and OH* was included, as previously considered for metal catalysts containing Cu, Pd and Zn.[20–22,24]

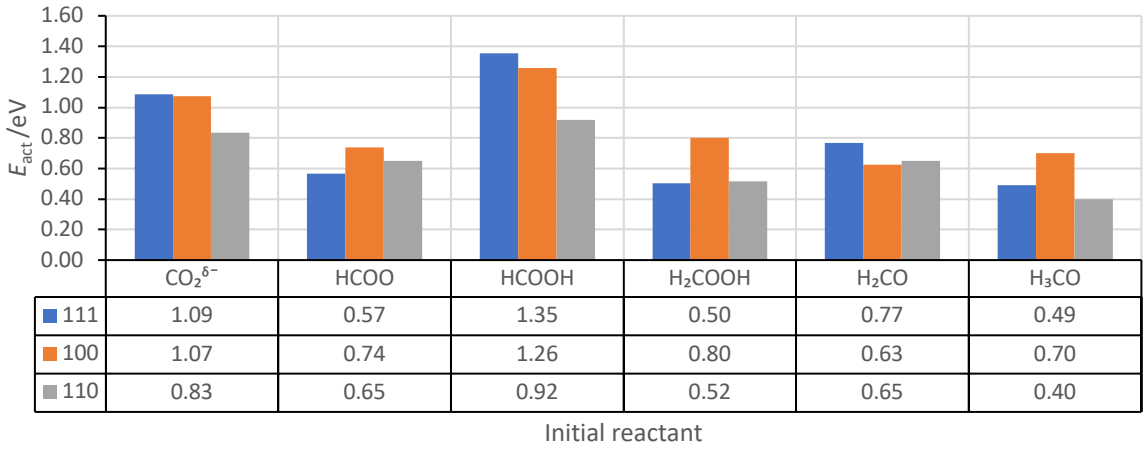

	$CO_2^{\delta-}$	HCOO	HCOOH	H_2COOH	H_2CO	H_3CO
111	1.09	0.57	1.35	0.50	0.77	0.49
100	1.07	0.74	1.26	0.80	0.63	0.70
110	0.83	0.65	0.92	0.52	0.65	0.40

Figure 12. The activation energies (E_{act}, eV) of reaction steps in the pathway for CO_2 hydrogenation to methanol, presented for Pd surfaces in order of increasing E_{surf} ,i.e. (111), (100), and (110), given in blue, orange, and grey, respectively. In each case, the label refers to the initial reaction species , and the activation energies are also tabulated.

The activation energy for $CO_2^{\delta-}$ hydrogenation, $E_{act}(CO_2^{\delta-})$, is 1.09 eV, 1.07 eV and 0.83 eV on the Pd (111), (100) and (110) surfaces, respectively. The observation that $E_{act}(CO_2^{\delta-})$ is lowest on the Pd (110) surface can be attributed to the additional space underneath the $CO_2^{\delta-}$ on the preferred long-bridge site, which facilitates the hydrogen atom binding to the carbon. The $E_{act}(CO_2^{\delta-})$ on the Pd (111) surface reported (1.09 eV) matches the work of Zhang *et al.* (0.85 eV), though differs somewhat from the results of Brix *et al.* (2.23 eV); we believe this difference stems from use of a physisorbed CO_2 geometry

in their calculations, i.e. an Eley-Rideal mechanism, with a chemisorbed structure considered in our work and the calculations by Zhang *et al*.[23,24]

E_{act}(HCOOH) is observed to decrease with increasing E_{surf}, i.e. follows the trend (111) > (100) > (110). The highest E_{act}(HCOOH) of 1.35 eV, calculated for the Pd (111) surface, is in good agreement with the value of 1.13 eV reported by Brix *et al.* Given that the adsorption energy of HCOOH on the Pd (111) surface is calculated as -0.67 eV, and desorption is considered as the reverse process, the high E_{act}(HCOOH) observed (1.35 eV) for the Pd (111) surface suggests that HCOOH is more likely to desorb than react further. The high activation barrier for HCOOH hydrogenation agrees with work by Huš *et al.* on Cu-based catalysts; however, formic acid is not amongst the product stream observed when using Pd catalysts experimentally, with CH_3OH, CO and trace to significant amounts of CH_4 reported.[6,15,16,21,45] Thus, another intermediate, such as H_2COO, might be of importance in leading to the experimental products, as was determined for Cu-based catalysts.[21]

The activation energy for dissociation of H_2COOH species, $E_{act}(H_2COOH)$, is highest on the Pd (100) surface, where the H_2COOH intermediate is stabilised. Brix *et al.* reported a very high $E_{act}(H_2COOH)$ of 2.01 eV on Pd (111), while we observe $E_{act}(H_2COOH)$ to be only 0.50 eV. For hydrogenation of formaldehyde, $E_{act}(H_2CO)$ is similarly low on the three surfaces; however, on the (111) surface it is very close to the E_{ads} of H_2CO, which again might result in desorption rather than hydrogenation.

In the majority of hydrogenation steps examined on all three Pd surfaces, the reaction pathway favoured migration of the hydrogen atom towards the least stable on-top site before bonding to the intermediate. Therefore, the relative stability of the hydrogen adsorption sites, as shown in the Section 3.1, has a major impact on the E_{act} for most hydrogenation reactions on the Pd (111), (100) and (110) surfaces. It is noted therefore that reducing the difference in stability for hydrogen atoms on the possible surface sites might be an important factor in the design of catalysts for CO_2 hydrogenation to methanol, as this could lead to reduction of E_{act} for species reacting on a Pd-based catalyst.

A reaction profile based on the energy of initial, TS and final geometries, relative to the energy of isolated Pd (111), (100) and (110) surfaces and gas-phase reactants, is plotted in Figure 13, with each individual step balanced stoichiometrically by energies of gas-phase molecules.

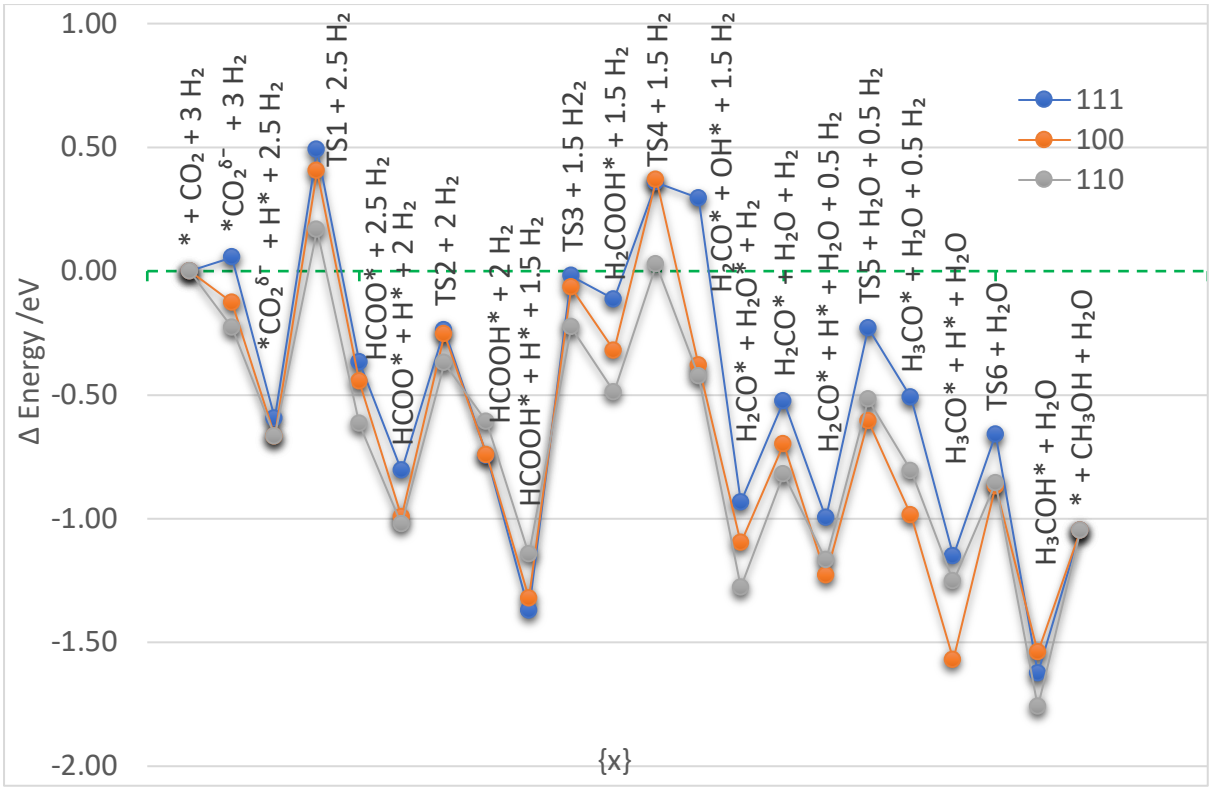

Figure 13. The energy profile of CO_2 hydrogenation to methanol, *via* the formate pathway, on Pd (111), (100), and (110) surfaces, plotted in blue, orange, and grey, respectively, relative to the energy of pristine surface and gas phase reactants.[22] Energies of intermediate structures and transition state geometries have been stoichiometrically balanced with energies of gas phase reactants; * indicates surface bound species.

Over all the surfaces, the conversion of CO_2 to methanol is exothermic relative to gas phase reactants, which agrees with experimental data.[6] The highest E_{act} in the CO_2 hydrogenation reaction across the Pd (111), (100) and (110) surfaces is E_{act}(HCOOH), with values of 1.35, 1.26, and 0.92 eV, respectively; thus, this is considered to be the rate determining step (RDS) of the reaction. An important feature of the reaction energy profile is that TS1 remains endothermic on all three surfaces, with respect to the gas phase reactants, which would inevitably influence the rate of the reaction. As highlighted in Section 3.1, the hydrogen atoms are stabilised strongly on the Pd (111), (100), and (110) surfaces; the binding energies of intermediates with a neighbouring hydrogen atom do not vary significantly from the sum of binding energies of the adsorbates calculated separately, which suggests that the presence of hydrogen neither stabilises nor destabilises the intermediates at the low monolayer coverage (1/9 ML) of hydrogen considered.[22]

4. **Summary and Conclusions**

Direct hydrogenation of CO_2 to methanol on transition metal catalysts is a promising way of green energy storage, and in order to make the technology viable, new and more efficient catalysts need to be designed. Here, we have investigated the CO_2 hydrogenation reaction *via* the formate pathway on Pd (111), (100), and (110) surfaces. The transition state for $CO_2^{\delta-}$ hydrogenation (TS1), to form formate, is endothermic, which will influence the overall rate of the reaction. E_{act}(HCOOH) is the highest energy step in the reaction profile on the Pd (111), (100), and (110) surfaces (TS3), and it can be considered as the rate determining step of this reaction on the surfaces examined. Novel Pd-based polymetallic nanoparticle catalysts for direct CO_2 hydrogenation to methanol could be designed to lower the barrier to initial CO_2 hydrogenation, TS1, and also lower the barrier for formic acid hydrogenation (TS3) or facilitate a mechanism that proceeds *via* an alternative intermediate, such as H_2COO.

This work provides a foundation for understanding the chemical reactivity of CO_2 on novel polymetallic Pd-based catalysts for direct CO_2 hydrogenation; further studies could involve investigating initial hydrogenation step proceeding via e.g. COOH; CO_2 dissociation to CO and O; and/or subsequent hydrogenations to HCO and H_2CO. The H_2COO intermediate could be alternatively considered as part of the formate pathway. Future work will entail modelling of the reaction on bimetallic and trimetallic Pd-based surfaces, which have been shown to manifest great selectivity to CH_3OH in direct CO_2 hydrogenation.[16,46–48]

5. **Acknowledgements**

The authors are grateful for funding by the EPSRC Centre-to Centre Project (Grant reference: EP/S030468/1). IK acknowledges the Cardiff School of Chemistry for a PhD studentship award. We are grateful to Matthias Scheffler, Yuanyuan Zhou, Herzain Rivera, Graham Hutchings, Mike Bowker and David Willock for useful discussions. AJL acknowledges funding by the UKRI Future Leaders Fellowship program (MR/T018372/1). The authors acknowledge computational resources and support from: the Supercomputing Wales project, which is part-funded by the European Regional Development Fund (ERDF) via the Welsh Government; the UK National Supercomputing Services ARCHER and ARCHER2, accessed via membership of the Materials Chemistry Consortium, which is funded by Engineering and Physical Sciences Research Council (EP/L000202/1, EP/R029431/1, EP/T022213/1); and the Isambard UK National Tier-2 HPC Service operated by GW4 and the UK Met Office, and funded by EPSRC (EP/P020224/1).

6. References

(1) Hutchings, G.; Davidson, M.; Atkins, P.; Collier, P.; Jackson, N.; Morton, A.; Muskett, M.; Rosseinsky, M.; Styring, P.; Thornley, P.; Williams, C. *Sustainable Synthetic Carbon Based Fuels for Transport: Policy Briefing*; The Royal Society, 2019.

(2) Roy, S.; Cherevotan, A.; Peter, S. C. Thermochemical CO_2 Hydrogenation to Single Carbon Products: Scientific and Technological Challenges. *ACS Energy Lett.* **2018**, *3* (8), 1938–1966.

(3) Bussche, K. M. V.; Froment, G. F. A Steady-State Kinetic Model for Methanol Synthesis and the Water Gas Shift Reaction on a Commercial Cu/ZnO/Al_2O_3Catalyst. *J. Catal.* **1996**, *161* (1), 1–10.

(4) French, S. A.; Sokol, A. A.; Bromley, S. T.; Catlow, C. R. A.; Rogers, S. C.; King, F.; Sherwood, P. From CO2 to Methanol by Hybrid QM/MM Embedding. *Angew. Chem. Int. Ed.* **2001**, *40* (23), 4437–4440.

(5) https://www.gov.uk/government/news/uk-becomes-first-major-economy-to-pass-net-zero-emissions-law (accessed Nov 28, 2019).

(6) Bowker, M. Methanol Synthesis from CO2 Hydrogenation. *ChemCatChem* **2019**, *11* (17), 4238–4246.

(7) Ko, J.; Kim, B.-K.; Han, J. W. Density Functional Theory Study for Catalytic Activation and Dissociation of CO2 on Bimetallic Alloy Surfaces. *J. Phys. Chem. C* **2016**, *120* (6), 3438–3447.

(8) Solymosi, F.; Berkó, A. Adsorption of CO2 on Clean and Potassium-Covered Pd(100) Surfaces. *J. Catal.* **1986**, *101* (2), 458–472.

(9) Solymosi, F. The Bonding, Structure and Reactions of CO2 Adsorbed on Clean and Promoted Metal Surfaces. *J. Mol. Catal.* **1991**, *65* (3), 337–358.

(10) Matsushima, T.; Asada, H. Kinetic Studies on the CO Oxidation on Pd(111) with Low Energy Electron Diffraction (LEED) and Angle-resolved Thermal Desorption. *J. Chem. Phys.* **1986**, *85* (3), 1658–1668.

(11) Burghaus, U. Surface Chemistry of CO2 – Adsorption of Carbon Dioxide on Clean Surfaces at Ultrahigh Vacuum. *Prog. Surf. Sci.* **2014**, *89* (2), 161–217.

(12) Kao, C.-L.; Carlsson, A.; Madix, R. J. The Adsorption Dynamics of Molecular Carbon Dioxide on Pt(111) and Pd(111). *Surf. Sci.* **2002**, *497* (1), 356–372.

(13) Liu, X.; Sun, L.; Deng, W.-Q. Theoretical Investigation of CO2 Adsorption and Dissociation on Low Index Surfaces of Transition Metals. *J. Phys. Chem. C* **2018**, *122* (15), 8306–8314.

(14) Erdöhelyi, A.; Pásztor, M.; Solymosi, F. Catalytic Hydrogenation of CO2 over Supported Palladium. *J. Catal.* **1986**, *98* (1), 166–177.

(15) Iwasa, N.; Suzuki, H.; Terashita, M.; Arai, M.; Takezawa, N. Methanol Synthesis from CO2 Under Atmospheric Pressure over Supported Pd Catalysts. *Catal. Lett.* **2004**, *96* (1), 75–78.

(16) Bahruji, H.; Bowker, M.; Hutchings, G.; Dimitratos, N.; Wells, P.; Gibson, E.; Jones, W.; Brookes, C.; Morgan, D.; Lalev, G. Pd/ZnO Catalysts for Direct CO2 Hydrogenation to Methanol. *J. Catal.* **2016**, *343*, 133–146.

(17) Ko, J.; Kim, B.-K.; Han, J. W. Density Functional Theory Study for Catalytic Activation and Dissociation of CO2 on Bimetallic Alloy Surfaces. *J. Phys. Chem. C* **2016**, *120* (6), 3438–3447.

(18) Habas, M.-P.; Mele, F.; Sodupe, M.; Illas, F. Density Functional Cluster Model Study of Bonding and Coordination Modes of CO2 on Pd(111). *Surf. Sci.* **1999**, *431* (1), 208–219.

(19) Medford, A. J.; Sehested, J.; Rossmeisl, J.; Chorkendorff, I.; Studt, F.; Nørskov, J. K.; Moses, P. G. Thermochemistry and Micro-Kinetic Analysis of Methanol Synthesis on ZnO (0001). *J. Catal.* **2014**, *309*, 397–407.

(20) Kattel, S.; Ramírez, P. J.; Chen, J. G.; Rodriguez, J. A.; Liu, P. Active Sites for CO2 Hydrogenation to Methanol on Cu/ZnO Catalysts. *Science* **2017**, *355* (6331), 1296–1299.

(21) Huš, M.; Kopač, D.; Štefančič, N. S.; Jurković, D. L.; Dasireddy, V. D. B. C.; Likozar, B. Unravelling the Mechanisms of CO2 Hydrogenation to Methanol on Cu-Based Catalysts Using First-Principles Multiscale Modelling and Experiments. *Catal. Sci. Technol.* **2017**, *7* (24), 5900–5913.

(22) Grabow, L. C.; Mavrikakis, M. Mechanism of Methanol Synthesis on Cu through CO2 and CO Hydrogenation. *ACS Catal.* **2011**, *1* (4), 365–384.

(23) Zhang, M.; Wu, Y.; Dou, M.; Yu, Y. A DFT Study of Methanol Synthesis from CO2 Hydrogenation on the Pd(111) Surface. *Catal. Lett.* **2018**, *148* (9), 2935–2944.

(24) Brix, F.; Desbuis, V.; Piccolo, L.; Gaudry, É. Tuning Adsorption Energies and Reaction Pathways by Alloying: PdZn versus Pd for CO_2 Hydrogenation to Methanol. *J. Phys. Chem. Lett.* **2020**, *11* (18), 7672–7678.

(25) Blum, V.; Gehrke, R.; Hanke, F.; Havu, P.; Havu, V.; Ren, X.; Reuter, K.; Scheffler, M. Ab Initio Molecular Simulations with Numeric Atom-Centered Orbitals. *Comput. Phys. Commun.* **2009**, *180* (11), 2175–2196.

(26) Larsen, A. H.; Mortensen, J. J.; Blomqvist, J.; Castelli, I. E.; Christensen, R.; Du\lak, M.; Friis, J.; Groves, M. N.; Hammer, B.; Hargus, C.; Hermes, E. D.; Jennings, P. C.; Jensen, P. B.; Kermode, J.; Kitchin, J. R.; Kolsbjerg, E. L.; Kubal, J.; Kaasbjerg, K.; Lysgaard, S.; Maronsson, J. B.; Maxson, T.; Olsen, T.; Pastewka, L.; Peterson, A.; Rostgaard, C.; Schiøtz, J.; Schütt, O.; Strange, M.; Thygesen, K. S.; Vegge, T.; Vilhelmsen, L.; Walter, M.; Zeng, Z.; Jacobsen, K. W. The Atomic

Simulation Environment—a Python Library for Working with Atoms. *J. Phys. Condens. Matter* **2017**, *29* (27), 273002.

(27) Ernzerhof, M.; Scuseria, G. E. Assessment of the Perdew–Burke–Ernzerhof Exchange-Correlation Functional. *J. Chem. Phys.* **1999**, *110* (11), 5029–5036.

(28) Tkatchenko, A.; Scheffler, M. Accurate Molecular Van Der Waals Interactions from Ground-State Electron Density and Free-Atom Reference Data. *Phys. Rev. Lett.* **2009**, *102* (7), 073005.

(29) Monkhorst, H. J.; Pack, J. D. Special Points for Brillouin-Zone Integrations. *Phys. Rev. B* **1976**, *13* (12), 5188–5192.

(30) Arblaster, J. W. Crystallographic Properties of Palladium. *Platinum Metals Rev.* **2012**, 56 (3), 181–189.

(31) Janthon, P.; Luo, S. (Andy); Kozlov, S. M.; Viñes, F.; Limtrakul, J.; Truhlar, D. G.; Illas, F. Bulk Properties of Transition Metals: A Challenge for the Design of Universal Density Functionals. *J. Chem. Theory Comput.* **2014**, *10* (9), 3832–3839.

(32) Methfessel, M.; Hennig, D.; Scheffler, M. Trends of the Surface Relaxations, Surface Energies, and Work Functions of the 4d Transition Metals. *Phys. Rev. B* **1992**, *46* (8), 4816–4829.

(33) Vitos, L.; Ruban, A. V.; Skriver, H. L.; Kollár, J. The Surface Energy of Metals. *Surf. Sci.* **1998**, *411* (1), 186–202.

(34) Patra, A.; Bates, J. E.; Sun, J.; Perdew, J. P. Properties of Real Metallic Surfaces: Effects of Density Functional Semilocality and van Der Waals Nonlocality. *Proc. Natl. Acad. Sci.* **2017**, *114* (44), E9188–E9196.

(35) Singh-Miller, N. E.; Marzari, N. Surface Energies, Work Functions, and Surface Relaxations of Low-Index Metallic Surfaces from First Principles. *Phys. Rev. B* **2009**, *80* (23), 235407.

(36) Da Silva, J. L. F.; Stampfl, C.; Scheffler, M. Converged Properties of Clean Metal Surfaces by All-Electron First-Principles Calculations. *Surf. Sci.* **2006**, *600* (3), 703–715.

(37) Skriver, H. L.; Rosengaard, N. M. Surface Energy and Work Function of Elemental Metals. *Phys. Rev. B* **1992**, *46* (11), 7157–7168.

(38) Tyson, W. R.; Miller, W. A. Surface Free Energies of Solid Metals: Estimation from Liquid Surface Tension Measurements. *Surf. Sci.* **1977**, *62* (1), 267–276.

(39) Boer, F. R. de; Mattens, W. C. M.; Boom, R.; Miedema, A. R.; Niessen, A. K. Cohesion in Metals. Transition metal Alloys. **1988**.

(40) Xantheas, S. S. On the Importance of the Fragment Relaxation Energy Terms in the Estimation of the Basis Set Superposition Error Correction to the Intermolecular Interaction Energy. *J. Chem. Phys.* **1996**, *104* (21), 8821–8824.

(41) Hansen, M. H.; Torres, J. A. G.; Jennings, P. C.; Wang, Z.; Boes, J. R.; Mamun, O. G.; Bligaard, T. An Atomistic Machine Learning Package for Surface Science and Catalysis. *ArXiv190400904 Phys.* **2019**.

(42) Henkelman, G.; Uberuaga, B. P.; Jónsson, H. A Climbing Image Nudged Elastic Band Method for Finding Saddle Points and Minimum Energy Paths. *J. Chem. Phys.* **2000**, *113* (22), 9901–9904.

(43) Conrad, H.; Ertl, G.; Latta, E. E. Adsorption of Hydrogen on Palladium Single Crystal Surfaces. *Surf. Sci.* **1974**, *41* (2), 435–446.

(44) Atkins, P.; de Paula, J. *Physical Chemistry*, 10th ed.; Oxford University Press, 2014.

(45) Fujitani, T.; Saito, M.; Kanai, Y.; Watanabe, T.; Nakamura, J.; Uchijima, T. Development of an Active Ga2O3 Supported Palladium Catalyst for the Synthesis of Methanol from Carbon Dioxide and Hydrogen. *Appl. Catal. Gen.* **1995**, *125* (2), L199–L202.

(46) Díez-Ramírez, J.; Valverde, J. L.; Sánchez, P.; Dorado, F. CO2 Hydrogenation to Methanol at Atmospheric Pressure: Influence of the Preparation Method of Pd/ZnO Catalysts. *Catal. Lett.* **2016**, *146* (2), 373–382.

(47) Díez-Ramírez, J.; Díaz, J. A.; Sánchez, P.; Dorado, F. Optimization of the Pd/Cu Ratio in Pd-Cu-Zn/SiC Catalysts for the CO2 Hydrogenation to Methanol at Atmospheric Pressure. *J. CO2 Util.* **2017**, *22*, 71–80.

(48) Bahruji, H.; Bowker, M.; Jones, W.; Hayward, J.; Ruiz Esquius, J.; Morgan, D. J.; Hutchings, G. J. PdZn Catalysts for CO_2 Hydrogenation to Methanol Using Chemical Vapour Impregnation (CVI). *Faraday Discuss.* **2017**, *197*, 309–324.